SECOND EUROPEAN CONFERENCE ON EARTHQUAKE ENGINEERING
AND SEISMOLOGY, ISTANBUL AUG. 25-29, 2014

BROADBAND STRONG GROUND MOTION SIMULATIONS OF LARGE SUBDUCTION EARTHQUAKES

Andreas A. SKARLATOUDIS[1] Paul G. SOMERVILLE[2] Hong Kie THIO[3] and Jeffrey R. BAYLESS[4]

ABSTRACT

The great interface earthquakes that occurred recently in the subduction zones of Peru, Chile and Japan have provided unparalleled information about the ground motions stemming from such earthquakes. Broadband ground motion simulations can enhance the usefulness of the recordings of these earthquakes by providing a means of interpolating and extrapolating the recorded data. Once they have been validated, broadband ground motion simulations can be used for forward predictions of the ground motions of great subduction events such as those in the Cascadia region. In this study, we show our capability to simulate, with a hybrid method, broadband strong motion recordings of mega-thrust earthquakes by demonstrating that our simulations reproduce the amplitudes of the recorded ground motions without systematic bias. We use simulations to study the distribution of various intensity measures of ground motion caused by these earthquakes, and validate our ground motion simulation method by comparing the simulated with recorded ground motions as well as with empirical ground motion prediction models. Finally, based on this evaluation, we use the method in a forward sense for computing the expected ground motions from a scenario **M** 9.0 mega-thrust earthquake that ruptures the entire Cascadia subduction zone.

INTRODUCTION

Ground motions from great subduction earthquakes make a large contribution to ground motion hazards in areas located in the vicinity of large subduction zones. In the United States Hazard Maps, the subduction source in the Pacific Northwest region is modeled by earthquakes having magnitudes as large as **M** 9.2. Since these magnitudes are larger than any of the earthquakes on which current empirical ground motion models (Atkinson and Boore, 2003; Zhao et al., 2006; Abrahamson et al., 2012) are based, it is important to use all the available information from the recent earthquakes in order to provide insight into the nature of ground motions from such large events.

The occurrence of the great subduction earthquakes in Peru, Chile and Japan provides the first glimpse at what the ground motions from such large earthquakes may be like. The **M** 8.4 Peru earthquake of June 23, 2001 was recorded at 8 strong motion stations, the **M** 8.8 Maule, Chile earthquake of February 27, 2010 was recorded at over twenty strong motion stations, while the **M** 9.0 Tohoku earthquake produced the most extensive data set of recordings for an earthquake of this magnitude. For the first time, data are available to guide the generation of ground motion scenarios from great subduction earthquakes. Broadband ground motion simulations can enhance the usefulness

[1] Seismologist, URS Corp, Los Angeles, andreas.skarlatoudis@urs.com
[2] Principal Seismologist, URS Corp, Los Angeles, paul.somerville@urs.com
[3] Principal Seismologist, URS Corp, Los Angeles, hong.kie.thio@urs.com
[4] Graduate Engineer, URS Corp, Los Angeles, jeff.bayless@urs.com

of the recordings of these earthquakes by providing a means of interpolating and extrapolating the recorded data.

The broadband ground-motion simulation method used in this study is based on the work of Somerville et al. (1991); Somerville (1993) and Graves and Pitarka (2004; 2010). It is a hybrid technique that computes the long and short period ranges separately and then combines the two to produce a single time history using appropriate matched filters. The method is relatively simple to apply since the only earthquake specific parameters needed as input are seismic moment, fault dimensions and geometry, hypocenter location, and a generalized model of the slip distribution. All other source parameters are determined using scaling relations. Recently the method has been applied for the first time for the simulation of an intraslab earthquake that occurred in California (**M** 6.5 2010 Ferndale earthquake). It reproduced the basic characteristics of the ground motions of this earthquake without systematic bias (Pitarka et al., 2013).

As described in detail below, we demonstrate the capability to simulate broadband ground motions from great subduction earthquakes and validate that capability by showing that it reproduces the amplitudes of the recorded ground motions of large earthquakes without systematic bias. Based on this validation, we apply the ground motion simulation procedures to estimate the ground motion characteristics of earthquakes that rupture the entire Cascadia subduction zone. We produce several different slip models and select the ones that could produce extreme and moderate ground motions in order to study their variability and sensitivity to the individual characteristics of the slip model. We compare the simulated ground motions with those predicted by other models, and make maps of the simulated ground motions for soft rock site conditions.

PROCEDURE FOR BROADBAND STRONG GROUND MOTION SIMULATION

The broadband ground-motion simulation method that is used in this study is based on the work of Somerville et al. (1991), Somerville (1993) and Graves and Pitarka (2004; 2010). It is a hybrid technique that computes the long and short period ranges separately and then combines the two to produce a single time history using appropriate matching filters. At periods longer than 1s, the methodology is deterministic and contains a theoretically rigorous representation of fault rupture and wave propagation effects. At periods shorter than 1s, it uses an empirical representation of source radiation and scattering derived from the recordings of a smaller earthquake.

The earthquake source is specified by a kinematic description of fault rupture, incorporating spatial heterogeneity in slip, rupture velocity and rise time. Following Hartzell and Heaton (1983), the fault is divided into a number of subfaults. The slip and rise time are constant across each individual subfault, although these parameters are allowed to vary from subfault to subfault.

The high frequency simulation methodology, used for periods usually shorter than 3.0s, is a semi-stochastic approach that sums the response for each subfault using empirical source functions. The simulation procedure was originally developed by Somerville et al. (1991) following the concepts of Irikura (1978) and Hartzell (1978). In this study, we use the Caleta de Campos rock site recording of an aftershock of the 1985 Michoacan, Mexico earthquake, described in detail by Cohee et al. (1991), which is combined with a simplified theoretical representation of wave propagation.

CASE STUDIES

We studied three large subduction earthquakes that occurred in the past 15 years. The **M** 8.4 Arequipa, Peru, the **M** 8.8 Maule, Chile and the **M** 9.0 Tohoku, Japan earthquakes produced large datasets of strong motion recordings. The source parameters of these earthquakes are listed in Table 1. The rupture model of the Arequipa, Peru, earthquake was derived by Somerville et al. (2003; 2008) and is shown in Figure 2. The rupture zone of the earthquake was about 400 km long, and most of the slip occurred in two asperities, one at shallow depths (5 - 15km) and the other at greater depths (25 - 40 km). The crustal velocity model that was used was derived from the results of Ocola et al. (1995). This model was modified to include a shallow layer of low seismic velocity representing weathered rock.

Table 1. Earthquake information and fault models adopted.

Name	Date	Origin Time	Lat (°)	Lon (°)	Depth (km)	M	Strike(°)	Dip(°)
Arequipa, Peru	2001/06/23	20:33:14	-16.140	-73.312	33	8.3	263	6
Maule, Chile	2010/02/27	06:34:14	-36.120	-72.900	35	8.8	9	12
Tohoku, Japan	2011/03/14	05:46:24	38.297	142.372	30	9.0	193	10

The earthquake rupture model of Lorito et al. (2011) was used to simulate the ground motions of the Maule, Chile earthquake. This rupture model, shown in Figure 3, was derived from both tsunami and geodetic data. The rupture zone of the earthquake was about 625 km along strike and 200 km down dip, and most of the slip occurred in two asperities, adjacent to the earthquake hypocenter at a depth about 35km. The crustal velocity model that was used is the same as used in the Arequipa simulations.

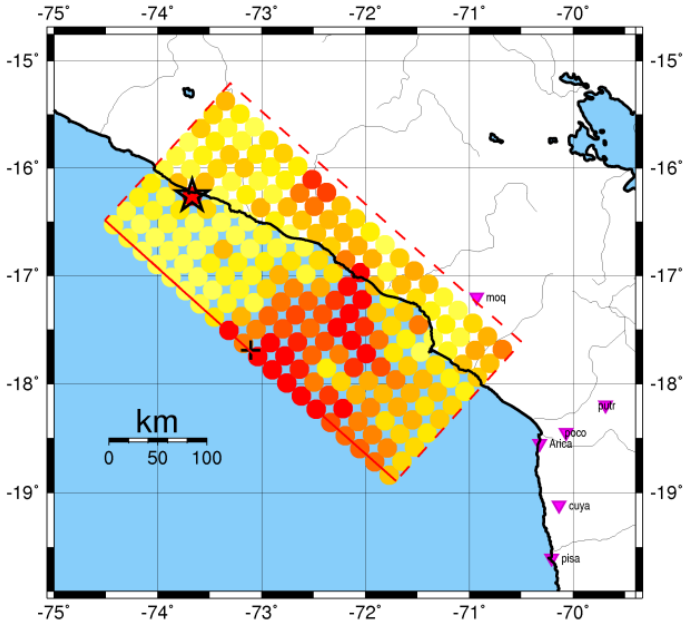

Figure 1. Rupture model of the M 8.4 2001 Arequipa, Peru earthquake and locations of strong ground motion recording stations.

Several rupture models have been proposed for the Tohoku, Japan earthquake, estimated using strong motion data (Kurahashi and Irikura, 2011), tsunami data (Fujii et al., 2011; Hayashi et al., 2011; Satake et al. 2012), geodetic data (Yue and Lay, 2011) and the combination of all these data (Koketsu et al., 2011; Yoshida et al., 2011;Yokota et al., 2011). In the present study we selected to use the rupture model of Kurahashi and Irikura (2011) (Figure 3) which contains five strong motion generating areas (SMGAs) with different sizes superimposed upon the larger rupture area of the earthquake. The total rupture area of the earthquake was about 480 km along strike and 150 km down dip. The stations selected for the comparison (triangles in Figure 3) are all fore-arc stations in order to avoid complex attenuation phenomena (Skarlatoudis and Papazachos, 2012; Stewart et al., 2013) and are part of the dataset that was used in deriving the Kurahashi and Irikura (2011) rupture model. The crustal structure model that we used for the simulations is based on the 3D velocity model for Japan derived by Koketsu et al. (2008). The 1D models for the various sites were extracted from the 3D model and the final model used in this study is an average of all those models.

An example of our evaluation of the simulated spectra is shown in Figure 4. For a subset of the recording sites of the 2011 Tohoku earthquake we compare the simulated spectra with the predictions of the Zhao et al. (2006) (Zhao06) and Abrahamson et al. (2012) (AGA12) ground motion models. The comparisons show that both models predict the recorded ground motions from this earthquake reasonably well, although there is a tendency to overpredict them, especially at the longer periods.

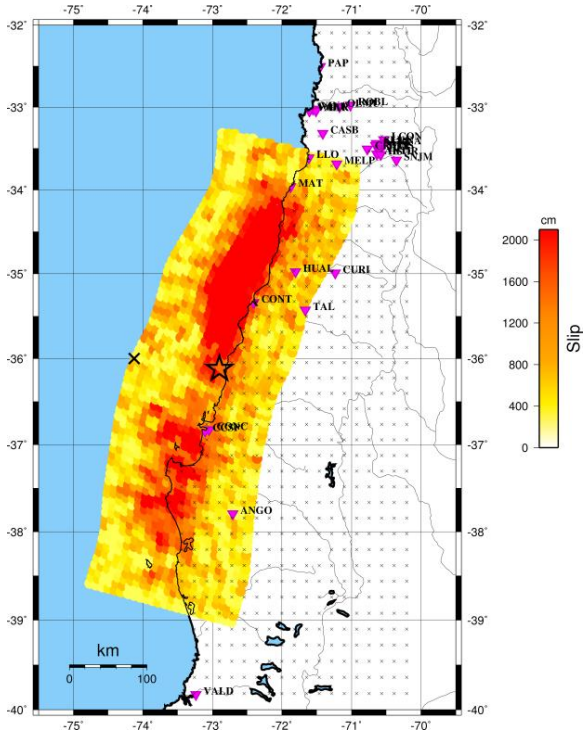

Figure 2. Rupture model of the M 8.8 Maule, Chile earthquake of 2010, showing the slip distribution of Lorito et al. (2011), the locations of strong ground motion recording stations (triangles), and the grid of stations used for simulations (grey dots).

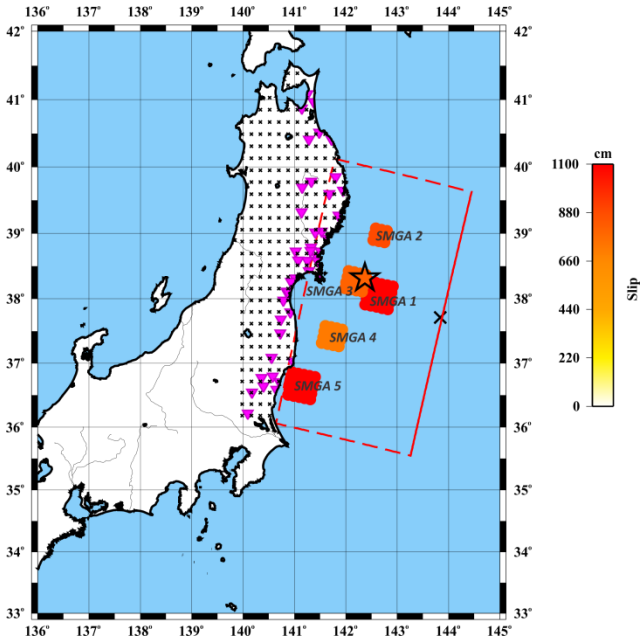

Figure 3. Rupture model of the M 9.0 Tohoku, Japan earthquake 2011, showing the slip distribution of Kurahashi and Irikura (2011), the locations of strong ground motion recording stations, and the grid of stations used for simulations.

GOODNESS-OF-FIT COMPARISONS

The comparisons between the recordings and the simulations at all stations for all three earthquakes studied are quantified in terms of response spectral goodness-of-fit (GOF). The residual between the observed and simulated spectral acceleration at a period T*i* for the j^{th} station is given by

$$r_j(T_i) = \ln[\frac{O_j(T_i)}{S_j(Ti)}] \quad (1)$$

where $O_j(T_i)$ and $S_j(T_i)$ are the observed and simulated values on a given component, respectively. The model bias is then given by

$$B(T_i) = \frac{1}{N}\sum_{j=1,N} r_j(T_i) \quad (2)$$

and the standard error is given by

$$\sigma(T_i) = \left\{\frac{1}{N}\sum_{j=1,N}\left[r_j(T_i) - B(T_i)\right]^2\right\}^{1/2} \quad (3)$$

following the notation of Graves and Pitarka (2010).

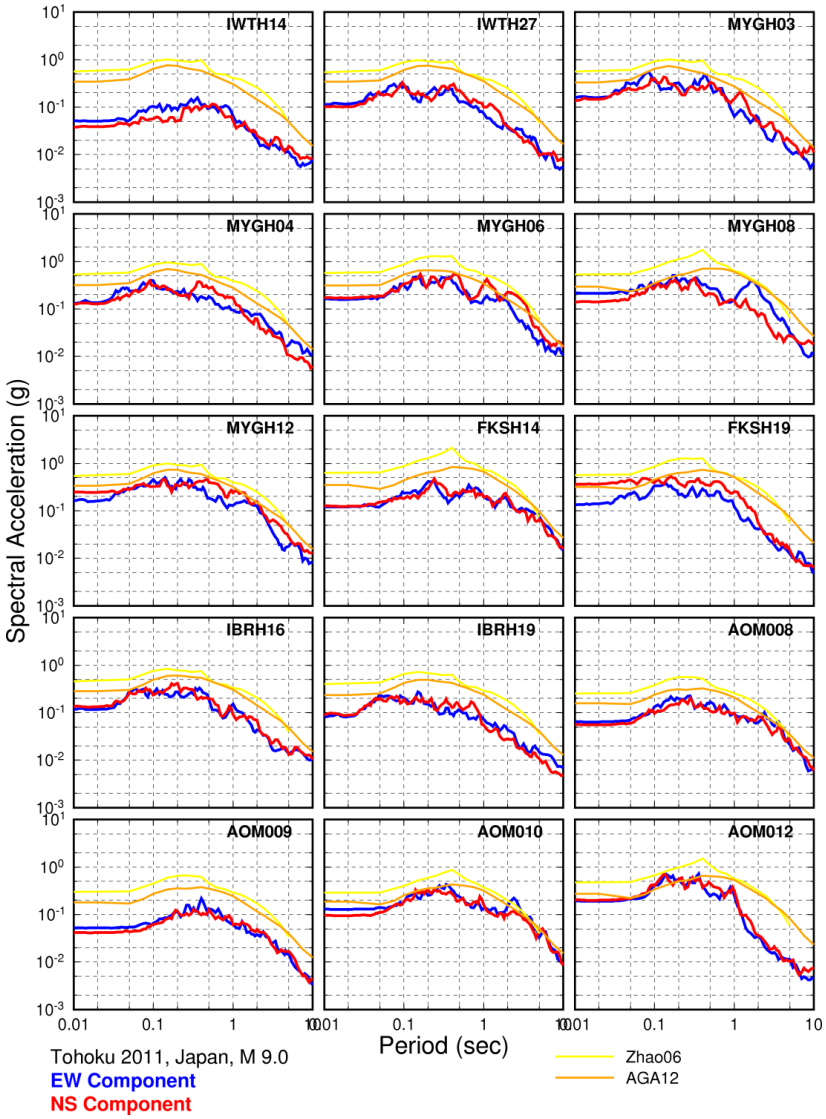

Figure 4. Comparison of the recorded response spectra of the 2010 Maule earthquake with the Zhao et al., 2006 and Abrahamson et al. (2012) ground motion prediction models.

The validation of our simulation method for the three case studies is given in Figure 5 which shows the spectral acceleration modeling bias (Equation 2). In Figure 5 the GOF plots for the average horizontal component of ground motion for the a) Arequipa, 2001, b) Maule, 2008 and c) Tohoku 2011 earthquakes are presented. The red line shows the bias; the light green zone shows the standard deviation, and the dark grey zone shows the 90% confidence interval of the mean. These comparisons

show little systematic bias in the prediction of the ground motions. The standard deviation of the prediction, shown by the grey shading, is about a factor of 1.5 (0.4 natural log units). The simulations have a model bias that is generally within 20% of zero across the full bandwidth. A systematic underprediction can be observed around the period of 0.5s. This underprediction could be driven by the characteristics of the empirical source function used in the high frequency part of the simulations.

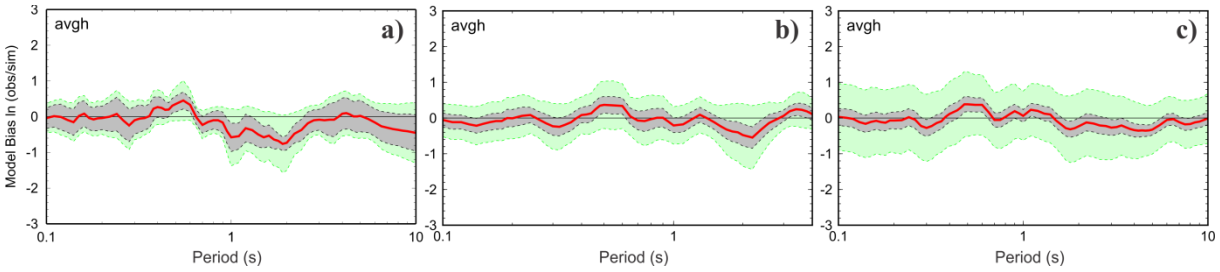

Figure 5. Goodness-of-fit (GOF) of recorded and simulated response spectra for a) the 2001 Arequipa, b) 2010 Maule and c) 2011 Tohoku earthquakes for the average horizontal component of ground motion. The red line shows the bias, the light green zone shows the standard deviation, and the dark grey zone shows the 90% confidence interval of the mean.

EARTHQUAKES THAT RUPTURE THE ENTIRE CASCADIA SUBDUCTION ZONE

Having validated our simulation methodology, we can now use it in many different ways with one of these being the simulation of subduction earthquake ground motions that rupture the entire Cascadia subduction zone. The fault geometry we used to represent the Cascadia subduction zone is shown in Figure 6.

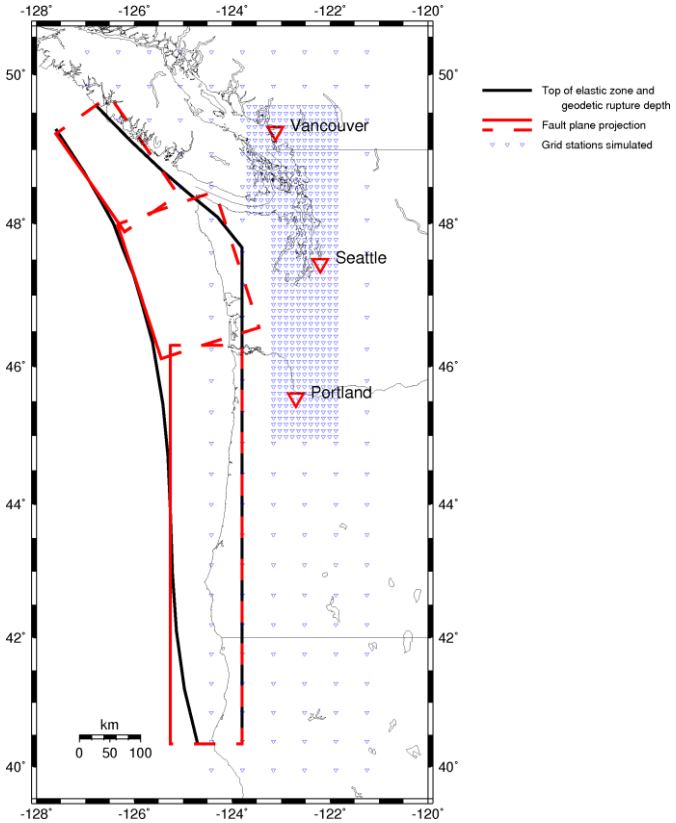

Figure 6. Modeled rupture geometry of the Cascadia subduction zone and the grid of stations used for strong motion simulation (blue triangles).

The subduction interface was divided into three segments to accommodate the shallower dip at the bend in the subduction zone near the Olympic Peninsula. The shallower segment has a downdip width of 160 km while the other segments have downdip widths of 120 km. The rupture area of the combined fault segments is 131,500 km^2. Based on the recent megathrust earthquakes that occurred worldwide, we performed simulations for an earthquake of magnitude **M** 9.0. The parameters of this event are shown in Table 2. Detailed information regarding the source characterization, the selection of the crustal model used and other parameters of the simulations can be found in Somerville et al. (2013).

Table 2. Source parameters of modeled **M** 9.0 earthquakes that rupture the whole Cascadia Subduction Zone.

M	Rupture Area (km^2)	Average Slip (cm)	Rise Time (s)	Slip Velocity (cm/s)
9.0	131,500	831	12.7	66.0

For this event, we generated more than 100 different earthquake rupture models, for three different hypocentral locations, i.e. south, central and north, in order to study the variability and the sensitivity of the derived ground motions to the individual characteristics of each slip model used. We selected three slip models for producing ground motion simulations. All the models have very similar average slip, although there are differences in the spatial distribution of slip, mostly in the down dip direction. For model 11 the slip is uniformly distributed along the fault, while for 27 and 87 the highest slip values are concentrated in the lower and upper parts of the fault, respectively. The rupture models of the **M** 9.0 event for the north hypocenter are shown in Figure 7.

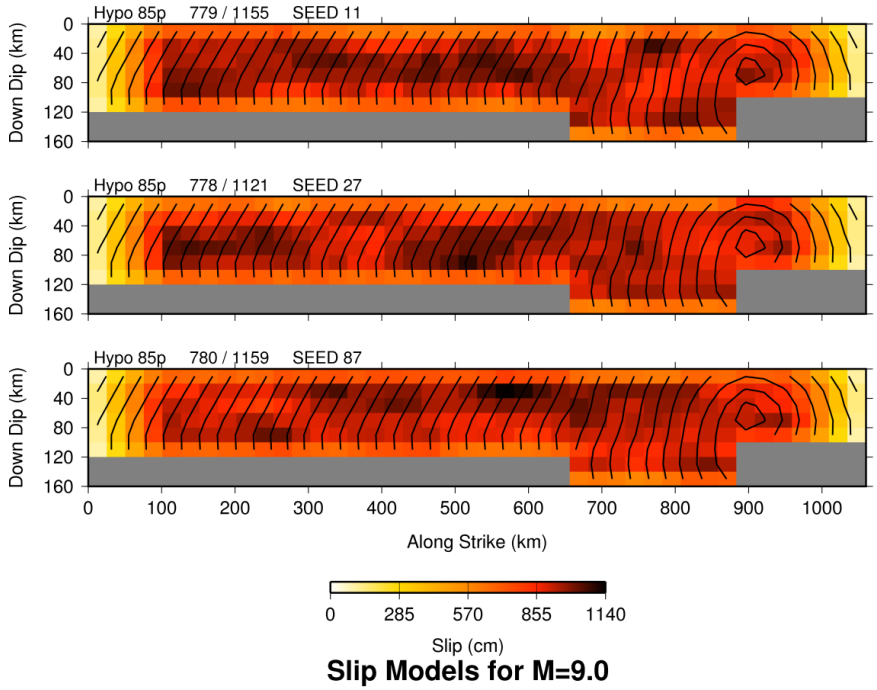

Figure 7. Rupture models of Mw 9.0 scenario earthquakes on the Cascadia subduction zone having northern hypocenters. The slip values of all models are the same for the different hypocenters (southern, central, and northern).

We performed ground motion simulations at the stations shown by the grid in Figure 6. The attenuation of ground motion with distance derived from the strong motion simulations is shown in Figure 8. At first the simple model described in Equation 4

$$\ln(Sa) = C_1 + C_2 * R_{cld} \quad (4)$$

is fit (shown by a solid black line) to the simulated ground motion values (the three different hypocentral locations are shown in different colors). The results are compared with the three ground motion models for PGA and 1s spectral period. The comparisons are presented for the NEHRP B/C boundary site condition. From Figures 8 and 9, it is clear that there are differences between the three ground motion models and our model, especially in the slopes of the attenuation curves. For close distances (R<50 km) there is fairly good agreement between the GMPEs and our model, which gradually improves with increasing periods. For larger distances, the three models underpredict the simulated ground motions, exhibiting stronger distance decay than our model, particularly at shorter periods, while for longer periods the results are in better agreement. In most cases the Atkinson and Boore (2003) model underpredicts the simulated response spectra, especially at closer distances, in agreement with the comparisons presented in the previous response spectrum comparisons. The Zhao et al. (2006) and Abrahamson et al. (2012) models are in closer agreement with our results, particularly for distances < 200km.

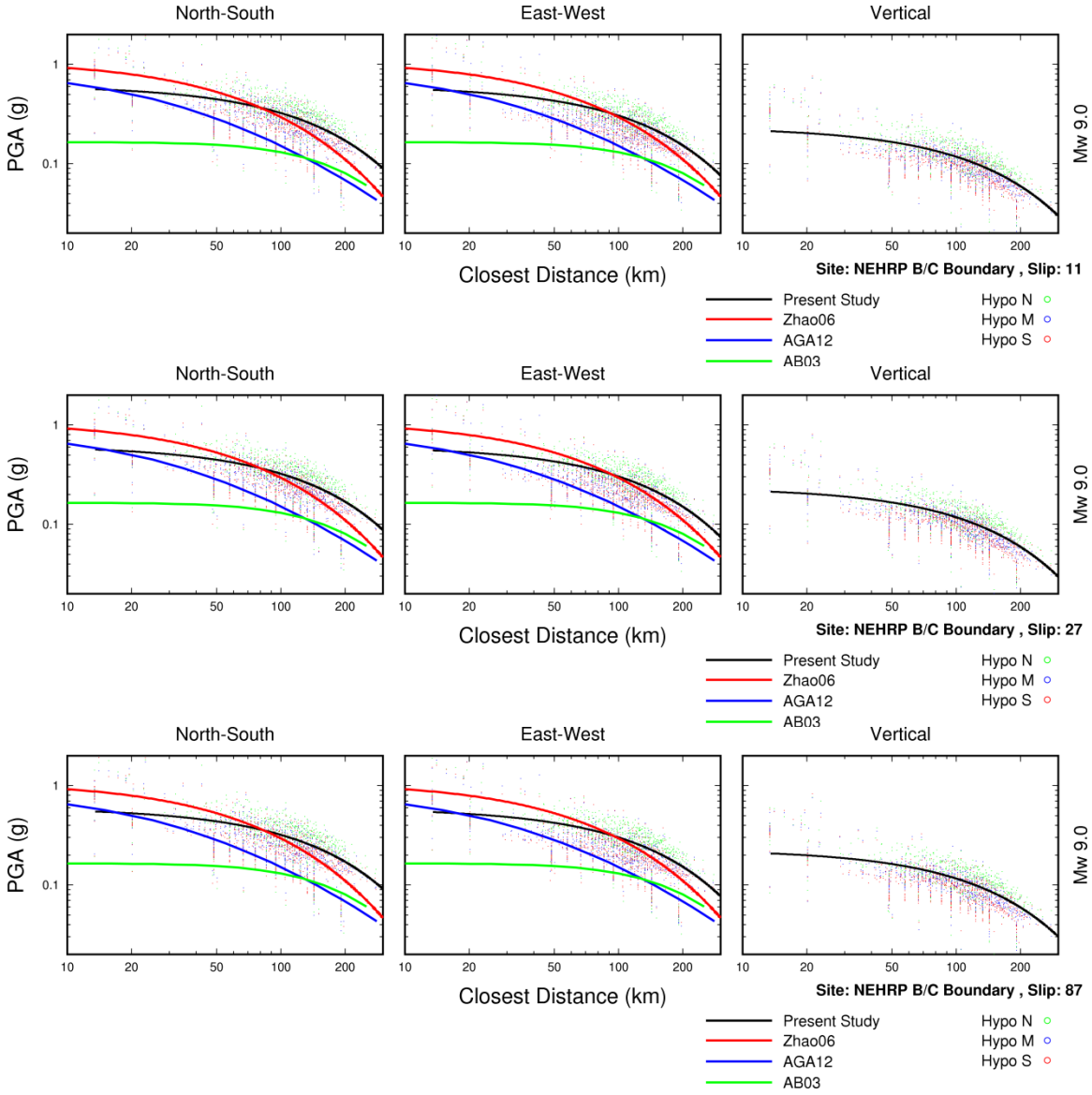

Figure 8. Comparison of simulated peak accelerations (points and black line), for various slip models for **M** 9.0 Cascadia earthquake with ground motion models for the NEHRP B/C site categories boundary.

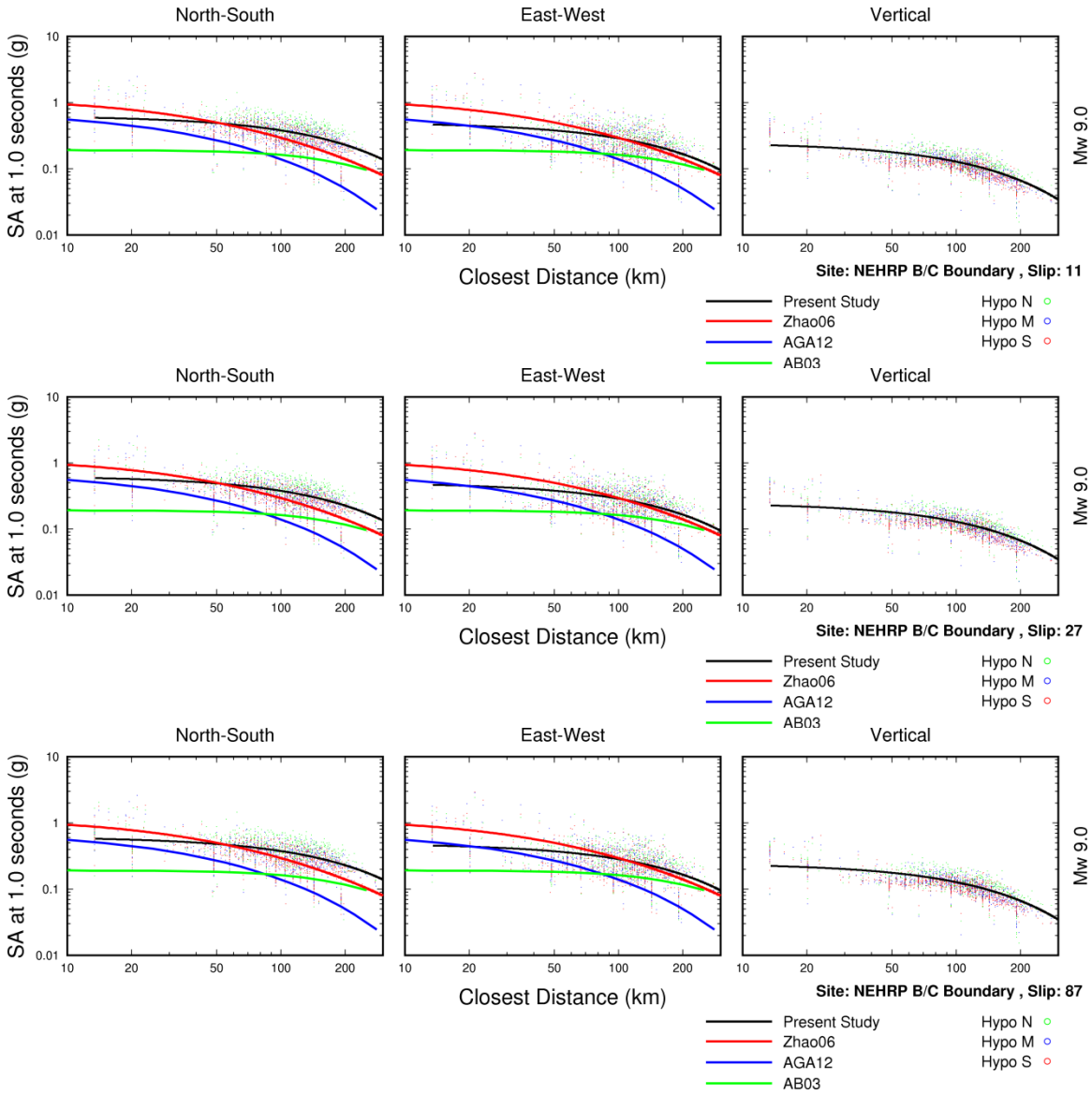

Figure 9. Comparison of simulated 1 sec spectral accelerations (points and black line), for various slip models for **M** 9.0 Cascadia earthquake with ground motion models for the NEHRP B/C site categories boundary.

We also generated ground motion maps for each of the three rupture scenarios. The maps, shown in Figure 10, are for peak acceleration for one of the three different slip models used (SEED 11) and for NEHRP B/C boundary site conditions.The highest values are observed in the broader area of the Olympic Peninsula, independent of the hypocentral location of the scenario earthquake.

DISCUSSION AND CONCLUSIONS

Figure 5 shows the spectral acceleration modeling bias for the three earthquakes we have examined. For all events the simulations have a model bias generally within 20% of zero across the full bandwidth. A systematic underprediction can be observed around the period of 0.5s in all three bias plots. This underprediction could be driven by the characteristics of the empirical source function used in the high frequency part of the simulations. The modeling standard error for spectral acceleration (from Equation 3) for the Tohoku earthquake along with corresponding measures computed from the four GMPE models used in the earthquake simulation evaluations is shown in Figure 11. The standard deviation for the Tohoku 2011 earthquake is fairly constant across the examined period range and comparable with the standard deviations of the most recent GMPE models (Zhao et al., 2006:Zea06 and Abrahamson et al, 2012:AGA12). The Atkinson and Boore (2003) (AB03) standard deviation is at

the lower bound of the standard deviations from the three simulations, while the Zea06 model has very comparable values for almost the whole period range examined.

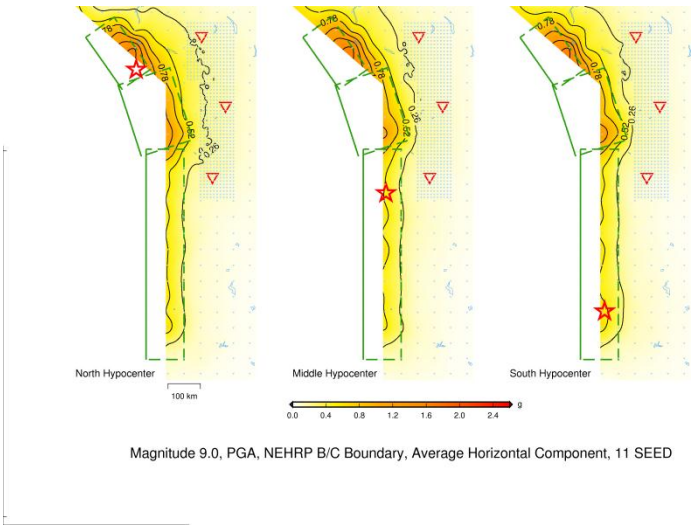

Figure 10. Ground motion maps for peak acceleration for an Mw 9.0 Cascadia earthquake for three hypocenter locations and various slip models, for NEHRP B/C boundary site conditions.

An example of the application of our simulation methods is shown in Figures 8 through 10. Figures 8 and 9 compare the forward simulations for a **M** 9.0 Cascadia earthquake with current GMPE models (AB03, Zea06 and AGA12) for different spectral periods (PGA and 1s). Larger variability can be observed for higher frequencies (PGA) which gradually diminishes at the period of 1s. Figure 11 shows an example of the generated ground motion maps for the same set of forward simulations. These maps show that the highest ground motions are observed in a broad area of the Olympic Peninsula, independent of the hypocentral location of the scenario earthquake. However, for the longer periods of ground motion (T>1s), the corresponding ground motions maps which are not shown here, indicate a well-defined coastal zone which extends from Washington to the northern parts of California with maximum values of ground motion.

Lay et al. (2012) have shown that for megathrust earthquakes, such as the one simulated for Cascadia, the spectral content of the recorded ground motions has depth varying characteristics, with the deeper ones producing ground motions richer in shorter periods and the shallower ones in longer periods, respectively. With the three different slip models that we have selected, we have tried to replicate this pattern and identify these properties in our simulations. As can be seen from Figures 8 through 10 as well as from other resutls not shown here, we cannot identify any significant differences in the simulated ground motions.

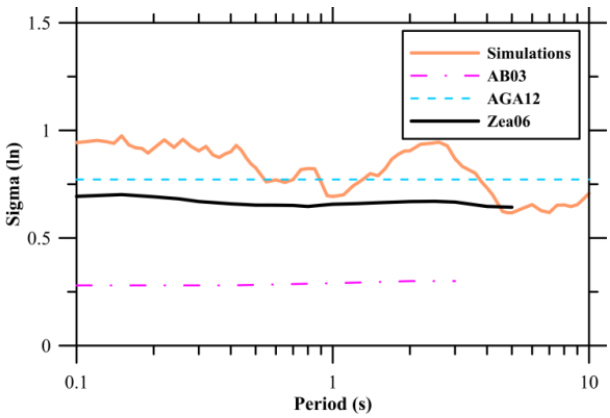

Figure 11. Comparison of spectral acceleration standard error for our simulations with that obtained from empirical ground motion prediction equations (GMPEs) for subduction areas. The AB03, Zea06, AGA12 GMPEs are used in the comparisons.

Considering the previous discussion, the validation results presented here demonstrate the ability of the hybrid simulation methodology to reproduce the main characteristics of the observed ground motions for interface earthquakes over a broad frequency range. Despite the various uncertainties in the presented comparisons it is obvious that broadband simulations can be useful in assessing certain characteristics of ground motions from mega-thrust earthquakes in subduction zones such as Cascadia that lack strong motion recordings of such events.

Acknowledgments

Research on the Maule and Tohoku earthquakes supported by the U.S. Geological Survey (USGS), Department of the Interior, under USGS award numbers (Paul Somerville, G11AP20041, G12AP20081). The views and conclusions contained in this document are those of the authors and should not be interpreted as necessarily representing the official policies, either expressed or implied, of the U.S. Government. Some plots were created using the Generic Mapping Tools version 4.2.1 (Wessel and Smith, 1998).

REFERENCES

Abrahamson N, N Gregor and K Addo (2012). BC Hydro Ground Motion Prediction Equations for Subduction Earthquakes. *Earthquake Spectra, submitted*.

Atkinson GM and DM Boore (2003). Empirical ground motion relations for subduction zone earthquakes and their application to Cascadia and other regions, *Bull. Seism. Soc. Am*. **93**, 1703-1729.

Cohee BP, PG Somerville and NA Abrahamson (1991). Ground motions from hypothesized Mw = 8 subduction earthquakes in the Pacific Northwest, *Bull. Seism. Soc. Am.* 81, 28-56.

Graves RW and A Pitarka (2004). Broadband time history simulation using a hybrid approach. Proceedings of the 13th World Conference on Earthquake Engineering, Vancouver, Canada, August 1-6, 2004, Paper No. 1098.

Graves RW and A Pitarka (2010). Broadband Ground-Motion Simulation Using a Hybrid Approach, *Bull. Seism. Soc. Am.* 100, 2095–2123.

Hartzell S (1978). Earthquake aftershocks as Green's functions. *Geophys. Res. Lett.* 5, 1-4.

Hartzell S, and T Heaton (1983). Inversion of strong ground motion and teleseismic waveform data for the fault rupture history of the 1979 Imperial Valley, California earthquake. *Bull. Seism. Soc. Am.*, 1553-1583.

Hayashi Y, H Tsushima, K Hirata, K Kimura, and K Maeda (2011). Tsunami source area of the 2011 off the Pacific coast of Tohoku Earthquake determined from tsunami arrival times at offshore observation stations, *Earth Planets Space* 63, 809–813.

Irikura K (1978). Semi-empirical estimation of strong ground motions during large earthquakes. *Bull. Disast. Prev. Res. Inst.*, Kyoto Univ. 63, 104.

Ishii TT Sato and PG Somerville (2000). Identification of main rupture areas of heterogeneous fault models for strong motion estimates. *J. Struct. Constr. Eng.* 527, 61-70.

Koketsu K, H Miyake, H Fujiwara and T Hashimoto (2008), Progress towards a Japan integrated velocity structure model and long-period ground motion hazard map, paper S10-038 presented at 14th World Conference on Earthquake Engineering, Beijing, China.

Koketsu K, Y Yokota, N Nishimura, Y Yagi, S Miyazaki, K Satake, Y Fujii, H Miyake, S Sakai, Y Yamanaka, T Okada (2011). A unified source model for the 2011 Tohoku earthquake, *Earth and Planetary Science Letters* 310, 480–487.

Kurahashi S and K Irikura (2011). Source model for generating strong ground motions during the 2011 off the Pacific coast of Tohoku Earthquake, *Earth Planets Space* 63, 571–576.

Lay T, H Kanamori, CJ Ammon, KD Koper, AR Hutko, L Ye, H Yue, TM Rushing (2012). Depth-varying rupture properties of subduction zone megathrust faults. Journal of Geophysical Research: Solid Earth doi:10.1029/2011JB009133.

Lorito S, F Romano, S Atzori, X Tong, A Avallone, J McCloskey, M Cocco, E Boschi and A Piatanesi (2011). Limited overlap between the seismic gap and coseismic slip of the great 2010 Chile earthquake. Nature Geoscience, 4, 173 – 177.

Ocola LC, J Luetgert, LT Aldrich, RP Meyer and CE Helsey (1995). Velocity structure of the coastal region of southern Peru from seismic refraction / wide-angle reflection data. *J. Geodynamics* 20, 1-30.

Pitarka A, HK Thio, P Somerville, and LF Bonilla (2013). Broadband Ground-Motion Simulation of an Intraslab Earthquake and Nonlinear Site Response: 2010 Ferndale, California, Earthquake Case Study. *Seis.* Res. *Lett.* 84, 785-795.

Satake K, Y Fujii, T Harada, and Y Namegaya (2012). Tsunami source model of the 2011 Tohoku earthquake and comparison with the 1896 Sanriku and 869 Jogan earthquakes, *Geophysical Research Abstracts* 14, EGU2012-3542-1, EGU General Assembly, 2012.

Skarlatoudis AA and CB Papazachos (2012). Preliminary study of Ground Motions of Tohoku, Japan Earthquake of March 11, 2011, *Seis. Res. Lett.* 83, 119-129.

Somerville PG (1993). Engineering applications of strong ground motion simulation, *Tectonophysics* 218, 195-219.

Somerville PG, MK Sen and BP Cohee (1991). Simulation of strong ground motions recorded during the 1985 Michoacan, Mexico and Valparaiso, Chile earthquakes, *Bull. Seism. Soc. Am.* 81, 1-27.

Somerville PG, T Sato, T Ishii, NF Collins, K Dan and H Fujiwara (2002). Characterizing heterogeneous slip models for large subduction earthquakes for strong ground motion prediction. Proceedings of the Architectural Institute of Japan.

Somerville PG, HK Thio, G Ichinose, N Collins, A Pitarka, and R Graves (2003). Earthquake source and ground motion characteristics of the June 23, 2001 Mw 8.4 Arequipa, Peru, earthquake. *Seism. Res. Let.* 74, 223.

Somerville P, R Graves and N Collins (2008). Ground motions from large Cascadia subduction earthquakes. Final Report, U.S. Geological Survey award.

Somerville P, A Skarlatoudis and W Li (2013). Ground motions and tsunamis from Mw 9.0 Cascadia subduction earthquakes based on validations using the Mw 8.8 Maule, Chile earthquake of 2010. Final Report, U.S. Geological Survey.

Stewart JP, S Midorikawa, RW Graves, K Khodaverdi, H Miura, Y Bozorgnia, and KW Campbell (2013). Implications of Mw 9.0 Tohoku-oki Japan earthquake for ground motion scaling with source, path, and site parameters, *Earthquake Spectra* 29 (S1), S1-21.

Wessel P, and HF Smith (1998). New, improved version of the generic mapping tools released, Eos Transactions AGU 79, 579.

Yokota Y, K Koketsu, Y Fujii, K Satake, S Sakai, M Shinohara, and T Kanazawa (2011). Joint inversion of strong motion, teleseismic, geodetic, and tsunami datasets for the rupture process of the 2011 Tohoku earthquake, *GRL* 38, doi:10.1029/2011GL050098.

Yoshida K, K Miyakoshi, and K Irikura (2011). Source process of the 2011 off the Pacific coast of Tohoku Earthquake inferred from waveform inversion with long-period strong-motion records, *Earth Planets Space* 63, 577–582.

Yue H and T Lay (2011). Inversion of high-rate (1 sps) GPS data for rupture process of the 11 March 2011 Tohoku earthquake (Mw 9.1), *GRL* 38, doi:10.1029/2011GL048700, 2011.

Zhao JX, J Zhang, A Asano, Y Ohno, T Oouchi, T Takahashi, H Ogawa, K Irikura, HK Thio, P Somerville, Y Fukushima, and Y Fukushima (2006). Attenuation Relations of Strong Motion in Japan using Site Classification based on Predominant Period. *Bull. Seism. Soc. Am.* 96, 898-913.